

Confocal

Airyscan

## The Airyscan Detector from ZEISS

Confocal Imaging with Improved Signal-to-Noise Ratio  
and Superresolution



We make it visible.

# The Airyscan Detector from ZEISS

## Confocal Imaging with Improved Signal-to-Noise Ratio and Superresolution

Author: Joseph Huff, Wolfgang Bathe, Dr. Ralf Netz  
Dr. Tiemo Anhut, Dr. Klaus Weisshart  
Carl Zeiss Microscopy GmbH, Germany

Date: July 2015

**With Airyscan, ZEISS introduced a new detector concept for confocal laser scanning microscopy (LSM). While traditional LSM designs use a combination of pinhole and single point detector, Airyscan is a 32 channel area detector and collects a pinhole-plane image at every scan position. Each detector element functions as a single, very small pinhole. Knowing the beam path and the spatial distribution of each of the 32 detectors enables very light efficient imaging with improved resolution and signal-to-noise. This paper explains how the detection concept is implemented in the ZEISS LSM 8 family.**

### Introduction

Over the last 25 years the technique of confocal imaging has grown to become the standard choice for most fluorescence microscopy applications. The increase in utilization of confocal imaging systems in basic biomedical research can be attributed to the ability of a confocal imaging system to produce optically sectioned images with high contrast while providing acquisition versatility to address many sample and application demands [1]. Most commercially available confocal imaging systems have over time developed novel approaches and options to increase image contrast and instrument versatility. However, what has not changed over time is the approach to creating the most fundamental aspect of a confocal imaging system: the creation of the optical section.

Traditionally, the optical sectioning ability of a confocal imaging system has been brought about by placing a field stop, the so-called pinhole, in a conjugate image plane in front of a detector along the fluorescence detection path. If the pinhole is sufficiently closed, out of focus light collected by the objective will be blocked from reaching the detector creating an optically sectioned image (Box 1). The concept of utilizing a pinhole in the detection pathway to block out of focus light was conceived by Marvin Minsky in 1955 in an effort to improve imaging of the central nervous system [2]. As a result, the foundation laid by Minsky's work has led to the growth and development of the laser scanning micros-

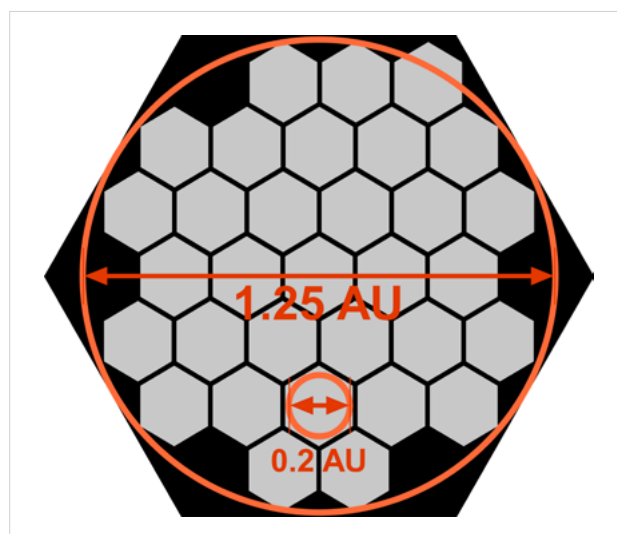


**Figure 1** Airyscan detector design. The Airyscan detector consists of elements that span an extensive area in the image plane. One element lies on the optical axis and acts like a classical point detector. The other elements are grouped around the center one, in a hexagonal pattern as shown in the example. Each detector element acts as a pinhole and will produce its own image. The image of the center detector element will be centered, whereas the images of the off-set detector elements will be displaced by approximately half their distance they have to the center. Hence, a detector array of 32 elements will produce 32 images with different displacements. As the sample is scanned, so will be the Airy disk of the point spread function (PSF) of a point emitter, which gives the detector and the method their names: Airyscan and Airyscanning, respectively. In the example each detector element acts as a pinhole of size 0.2 Airy units (AU); yet the whole detector area captures light of 1.25 AU. The 0.2 AU determines the sectioning and resolution in  $xy$  and  $z$ , whereas the 1.25 AU determines the sensitivity. By shifting back all the images to the center position, which can be easily done since the amounts of their displacements are known, an image called the "Sheppard sum" is generated, which itself has already higher resolution compared to a classical confocal. Deconvolution would further boost resolution information.

copy (LSM) over the past 25 years (The LSM 8 family is ZEISS's 8<sup>th</sup> generation of LSMs). As confocal systems developed and improved over this time, the constant hallmark of every commercial laser scanning confocal system has been the utilization of a physical aperture for a pinhole in combination with a unitary detector (typically a PMT). However, with the recent development and market introduction of the Airyscan detector from ZEISS, the traditional pinhole and detector design have been reworked to offer greatly improved resolution and signal-to-noise ratio (SNR). Introduced in 2014, the Airyscan detector replaces the physical confocal pinhole aperture and unitary detector assembly with a hexagonally-packed detector array. Just like the traditional confocal pinhole, the Airyscan detector is positioned in a conjugate focal plane to the excitation spot and utilizes a zoom optic arrangement to project a defined number of Airy unit orders onto the detector to create an optical section. By collecting the additional information of a pinhole-plane image at every excitation scan position, the Airyscan detector offers substantial and immediate benefit compared to traditional confocal microscopy by increasing both the signal-to-noise ratio and spatial resolution of all formed images, while maintaining the optical sectioning ability of a traditional confocal microscope. (Fig. 1) [3].

The idea of utilizing pinhole-plane image detection to improve spatial resolution and detection efficiency was first proposed around the same time the LSM market started to grow. In 1987 Bertero [4] and in 1988 Sheppard [5] both described approaches for pinhole-plane imaging systems. Much more recently, 2013, Sheppard et al. described the extension of so called pixel-re-assignment technique to fluorescent dyes [7]. However, until the introduction of the Airyscan detector, the idea of pinhole-plane image detection had yet to be adopted in a commercially available confocal laser scanning system. The following sections will outline and explain how the Airyscan detector hardware is implemented and describe how the resolution and SNR increase is achieved and how it compares to traditional laser scanning microscopy imaging.

### Limits of confocal microscopy

The introduction of a pinhole in a conjugate image plane was used to improve the optical sectioning capabilities of a scanning microscope by rejecting out of focus light. In addition to improving the optical section of an image closing the

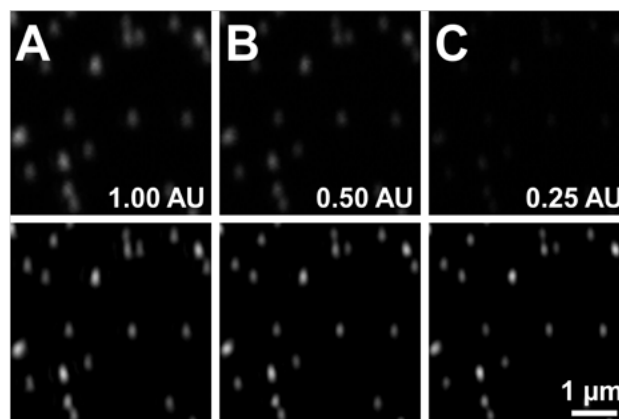


**Figure 2** Imaging with different pinhole sizes. (Upper panel) 100 nm TetraSpeck<sup>TM</sup> fluorescent microspheres (Thermo Fisher Scientific) were imaged at 488 nm at constant power and sampling rate (4x averaging) with pinhole sizes of 1.00 AU (A), 0.5 AU (B) and 0.25 AU (C). Relative sensitivities were 1.00 (a), 0.62 (B) and 0.27 (C). (Lower panel) The same beads were imaged again at the same pinhole settings, only this time laser powers were adjusted to yield the same sensitivity. Relative laser powers were 1.0 (A), 4.0 (B) and 65.0 (C).

pinhole holds the potential additional benefit of increasing the lateral and axial resolution of the resulting image. Traditionally the pinhole is set to the standard size of 1 Airy unit (1 AU). This already improves the spatial resolution compared to wide-field imaging by a typical factor of 1.06. The resolution can be further improved by closing the pinhole even further. But this comes at the price of a drastic reduction of valuable emission light that reaches the detector (Fig. 2) [5] (Box 2). The full resolution potential of a laser scanning confocal microscope, which is an enhancement by a factor of 2, can only be achieved theoretically: if the pinhole is completely closed.

Further, like all fluorescence imaging techniques, image quality in point scanning confocal microscopy is directly related to the ratio of the amount of signal (i.e. photons) and the amount of noise in an image (SNR). In point scanning confocal microscopy the detected photon numbers (signal) are generally extremely small due to labeling densities and/or the optical section created by the pinhole. The resulting statistic variation in the number of detected photons, the so called shot noise or photon noise, will then become a dominant factor for image contrast, i.e. the available grey levels per image pixel. As shot noise follows Poisson statistics, it will be equal to the square root of the signal. Hence, the SNR will also be proportional to the square root of the signal or synonymous to the square root of the number of photons (N):  $SNR \sim \sqrt{N}$ .

Another source of statistical noise is background fluorescence originating from out-of-focus signals and auto-fluorescence from the specimen or optical components. Both will limit the contrast of the signal in respect to the background and decrease the image SNR such that insufficient contrast exists for sample signals to be distinguished. The signal-to-background ratio (SBR) can be increased by closing the pinhole and would indeed be greatest if the pinhole aperture would be closed to zero. It is evident that this is not practical as the fluorescence signal would also be excluded from reaching the detector. Therefore a pinhole aperture size must be chosen to maximize image SNR while retaining an adequate SBR to yield a good image contrast. A pinhole size of 1 Airy unit (AU) has traditionally proven to be a good compromise to achieve this goal.

Imaging with a confocal microscope is always a trade-off between speed (sampling frequency), sensitivity (sampling frequency & pinhole size) and resolution (pinhole size) at a certain image SNR. For a given optical setup (and sample) improving on one of these parameters will always come at the cost of one or both of the others. This fact is symbolized by the eternal triangle of compromise (Fig. 3) [6].

If speed, for example, is increased to increase image acquisition rates, the sampling period or pixel dwell time has to be shortened. In consequence, less photons can be collected and sensitivity will drop. Likewise, if the pinhole is closed to enhance resolution, less light reaches the detector resulting again in a reduced sensitivity. On the other hand, if the pinhole is opened to increase sensitivity, resolution will be lost. Improving on all parameters simultaneously or on one parameter without a deterioration of the others parameters can only be achieved by increasing the number of detected photons and hence SNR. Traditionally the increase in detected photons has been achieved by either increasing the illumination laser power or by improving the collection efficiency of the detector. Increasing the illumination laser power has significant limitations in fluorescence microscopy. First, all fluorophores have quantum efficiency (QE) and photo-stability properties that dictate how many photons a fluorophore can emit and for how long. If too much excitation laser power is used, a fluorophore will be driven into a saturation state resulting in a limited photon flux. In addition, dependent on their stability, fluorophores might rapidly photo-bleach when driven into saturation, which induces phototoxicity when dealing with live samples.

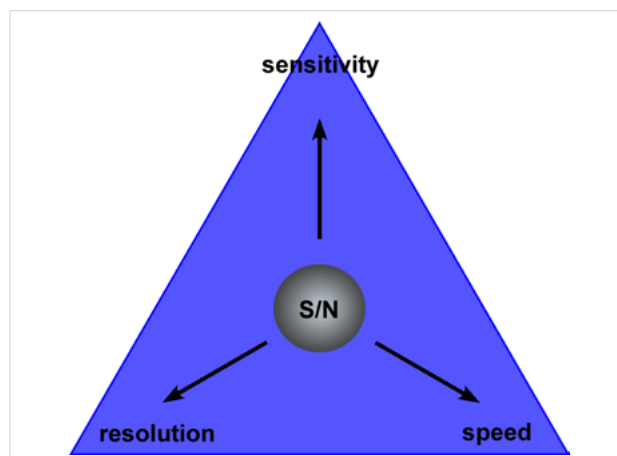


**Figure 3** The eternal triangle of compromise. The triangle states that for a given SNR, improving on one corner (resolution, speed or sensitivity) will inadvertently come at the cost of any of the other corners. In other words, the photon budget is divided between speed, sensitivity or resolution. Improvement in all corners can only be achieved, if the photon number or SNR can be increased.

A more viable approach to increase the SNR of an image has been to increase the QE of the unitary PMT detector typically used in scanning confocal imaging systems. Gallium Arsenide Phosphide Photomultiplier Tubes (GaAsP-PMT) yield, for example, superior SNR over Multialkali (MA)-PMTs without compromising on speed and resolution. Over the past five years the use of GaAsP PMTs for confocal microscopy has become a standard. With the introduction of the Airyscan detector from ZEISS there is now a third option available. It delivers even better image quality than traditional GaAsP confocals.

### Design of the Airyscan detector

The Airyscan detector consists of a hexagonal micro lens array that delivers light to 32 high transmission optical fibers. They are arranged in a hexagonal array on the light incident end and in a linear array on the light exiting end, respectively (Fig. 4) (Box 3). This efficient design delivers more than 95% of the emission light to the linear GaAsP-PMT detector array of the Airyscan detector.

The amount of light projected onto the detector, i.e. the size of the optical section used, is controlled by the zoom optics in front of the fiber bundle. The zoom optics project 1.25 AU onto the detector. Since the diameter of the Airyscan detector comprises 6 detector elements, each detector element represents a pinhole of the size of the imaged Airy disk divided by 6. Hence, if the zoom optics are set to capture 1.25 AU, the single detector elements act as pinholes with a size of  $1.25 \text{ AU}/6 \approx 0.2 \text{ AU}$ .

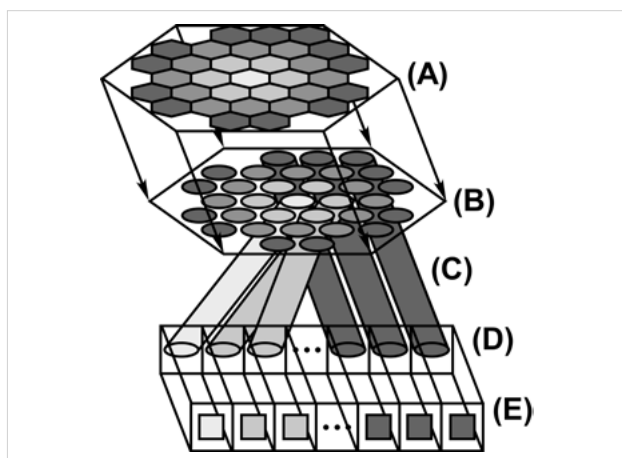


**Figure 4** Design of Airyscan detector. Incident light is collected by a hexagonal micro lens array (A) that connects directly to the ends (B) of a fiber bundle (C) as indicated by the arrows. The other ends (D) of the fibers are in contact to a linear GaAsP-PMT array (E), which is used as the detector in the proper sense. In this way, an area detector is created, onto which the Airy disk is imaged via a zoom optics. This allows to adapt the extent (in AU) of the Airy disk that is captured. The extent corresponds to the size of the physical pinhole in standard confocal microscopy and defines the amount of light that reaches the detector. Note that the classical pinhole is not needed for Airyscan detection, as the single detector elements act as separate pinholes.

As each detector element represents a small pinhole, the data collected by each element will yield a traditional confocal image. However, the properties of the images collected by the individual elements are slightly different. The central element for example will give the same image as a traditional LSM with a pinhole setting of 0.2 Airy units. All the other elements give images that are shifted laterally by app.  $\frac{1}{2}$  of the distance to the central element. Since the geometry of the Airyscan detector is well characterized, the relative positional information from each detector element can be used in two different ways to form a resulting image with increased resolution and SNR.

The easiest way to use the positional information from each detector element is to compensate for the image shifts induced by the displaced detector elements and then sum all the intensities. The resultant image has been termed the Sheppard Sum image, since it uses the properties found by Sheppard et. al.[5][7]. The Sheppard Sum image shows an improved lateral resolution of about 1.4 x laterally with no effect on axial resolution (Fig. 5). The sectioning capability of the Sheppard Sum Image is the same as for a conventional confocal image of the same total pinhole size. This can be easily seen: By reallocating intensities laterally, the overall intensity in a certain plane will not change. So the out-of-focus light intensity will also remain unaltered.

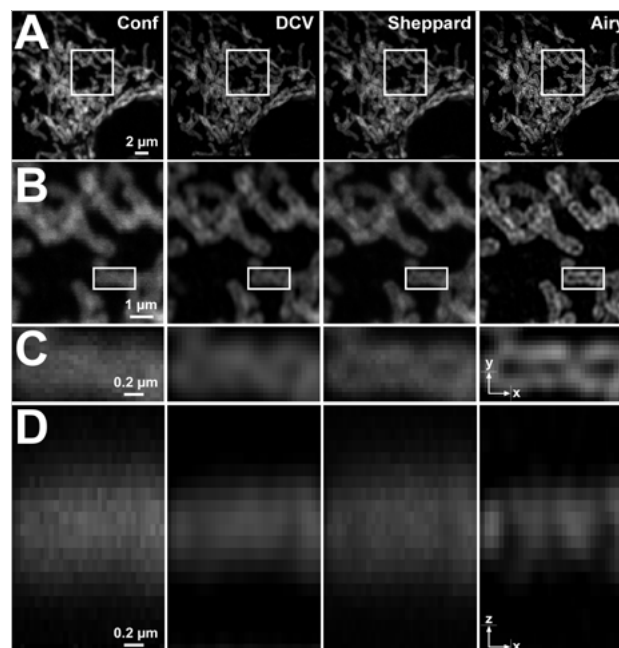


**Figure 5** The Sheppard sum. Sample is BSC-1 cells stained for TOMM 20 with antibodies conjugated to Alexa 568. (A) overview image; (B) zoomed area boxed in panel A; (C) zoomed area boxed in panel B in xy view. (D) Same area as in panel C, but in xz view. The Airyscan detector generates for each detector element a whole image that are slightly displaced against each other (phase images). By just summing up all images, a confocal equivalent image will be obtained (Conf). Deconvolution of the confocal image using the Airyscan deconvolution algorithm will improve contrast (DCV). However, by reassignment of the images to their correct position and summing all signal contributions at the reassigned site, the Sheppard sum image is generated that contains higher frequency information (Sheppard). These higher frequencies can be used by the Airyscan DCV algorithm for a more robust calculation yielding higher contrast (Airy). As in the Sheppard sum axial information is lost, no improvement in z-resolution is possible (compare Conf with Shepard in panel D). If however the single images are deconvolved separately and then their weighted sum deconvolved, z-resolution can be enhanced as well (compare DCV with Airy in panel D).

A more sophisticated way of utilizing the positional information of each detector element is to apply a DCV to each individual image collected by each detector element. Once each image has been deconvolved separately, the resulting image is weighted to acknowledge the detectors positional information and unique optical transfer function (OTF) to form a reconstructed sum image. By first deconvolving each image separately, the sectioning properties will improve beyond that of the traditional Sheppard Sum and the resulting imaging will have an enhanced z-resolution as well. Thus, a DCV step at the level of each detector element before the Sheppard Sum process results in a resolution improvement by a factor of 1.7 x in all three spatial directions is achieved.

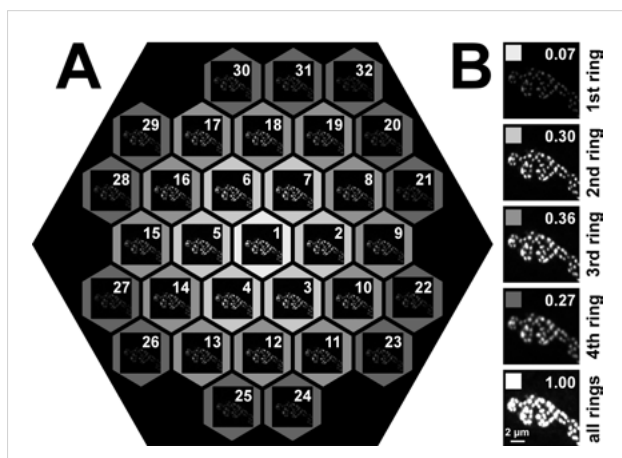


**Figure 6** Image formation in Airyscan. (A) Each detector element, numbered in the diagram from 1 to 32, acts as its own pinhole and records a complete image. The images are offset from the center. Groups of detector elements form rings that are indicated from inside to outside with increasingly darker grey shadings. The central ring (1st ring,  $\sim 0.2$  AU) consists of one element (#1), the next outward two rings (2nd and 3rd rings,  $\sim 0.6$  AU and  $\sim 1.0$  AU) of 6 (#2-7) and 12 (#8-19) elements, respectively, whereas the outer ring (4<sup>th</sup> ring,  $\sim 1.25$  AU) is formed by 13 elements (#20-32). From inside to outside detector elements or rings collect increasingly less light indicated by the progressively darker shading. However, the summed contribution of the outer rings to the total signal can be significant, especially for optically denser samples as shown in the example. (B) Intensity contribution of the different rings (sum of all respective detector elements of a ring). The numbers give the fraction of the total intensity (all rings summed). The sample is *Drosophila melanogaster* larval sections stained for the pre-synaptic protein Bruchpilot (Brp) with Alexa 488 and kindly provided by Jan Pielage, Friedrich-Miescher-Institute (FMI), Basel, Switzerland.

### Implications of increased SNR in Airyscan

The geometry of the Airyscan detector provides (and exceeds with deconvolution) the resolution benefits of a closed 0.2 AU pinhole with the light collection efficiency of a 1.25 AU pinhole. In this manner the resulting image SNR is drastically improved when comparing to traditional confocal imaging with a 0.2 AU pinhole. Further, when using the Airyscan the combination of detector elements and knowing the detector elements positions relative to the optical axis also offers the ability to dramatically improve the resolution and SNR when compared to imaging with the traditional 1 AU pinhole. The improvement in SNR is directly related to two effects: First, the larger overall pinhole size of 1.25 Airy Units collects up to 50% more light than the conventional 1 AU pinhole. Especially in optically denser specimens the contribution of this light to image formation can be substantial (Fig. 6). And secondly, the small individual pinholes not only show an extended resolution beyond an conventional LSM's resolution limit, but also raise the contrast of higher spatial frequencies collected by confocal microscope system

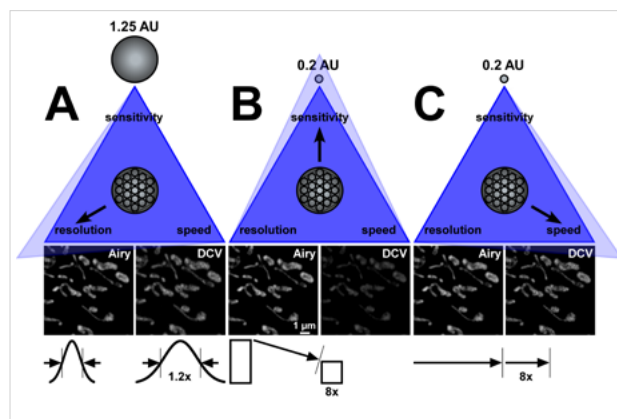


**Figure 7** Utilization of SNR gain in Airyscanning. Fluocells #1 (Thermo Fisher Scientific) were imaged for mitochondria stained with Mitotracker orange using a Plan Achromat 63x / oil 1.4 objective lens and 561 nm excitation line at 0.2%. One plane was recorded. Image conditions for Airyscan were as follows: resolution 524 x 524, pixel (px) size 0.047  $\mu\text{m}$ , pinhole 1.25 AU, sampling rate 2.02  $\mu\text{s}/\text{px}$ . Variations for confocal in (A) none; (B) pinhole 0.2 AU; (C) pinhole 0.2 AU, sampling rate 16.16  $\mu\text{s}/\text{px}$  by 8x line wise mean averaging. Deconvolutions on confocal images were performed with regularized inverse filtering excluding a Stokes-vector. In (A) image conditions in the confocal were kept identical to Airyscan to keep sensitivity and speed equal. Under these conditions the resolution achieved with Airyscan was about 1.2x higher than the deconvolved confocal as indicated. In (B) the pinhole size for the confocal was set to 0.2 AU keeping the sampling rate constant in order to keep resolution and speed equal to Airyscan. The Airyscan image showed approximately 8x higher sensitivity (intensity) compared to the deconvolved confocal. In (C) a pinhole size of 0.2 AU was set for the confocal and the sampling rate was reduced to 16.16  $\mu\text{s}$  per pixel in order to match the resolution and the sensitivity of Airyscan. This implies an 8 fold higher speed for Airyscan as indicated.

[5][7]. In other words, the Airyscan detector gives improved contrast without increasing noise, which directly translates to a substantial SNR increase in the final image.

The gain in SNR achieved by the Airyscan detector does not require any compromise in regards to speed, resolution or sensitivity. However, to have the same SNR at its disposal a traditional confocal has to compromise on speed, resolution or sensitivity (or combinations of those), which is an immediate consequence from the theory of the eternal triangle. If acquisition speed and sensitivity should match that of the Airyscan the pinhole has to be opened to 1.25 AU, which will result in lower resolution (Fig. 7). Likewise, if resolution and speed should equal Airyscan at otherwise identical settings, the pinhole would have to be set to 0.2 AU reducing light level and hence sensitivity. Finally, when resolution and sensitivity should be kept equal, again the pinhole has to be set to 0.2 AU to keep resolution and the sensitivity has to be increased by slower scanning or averaging.

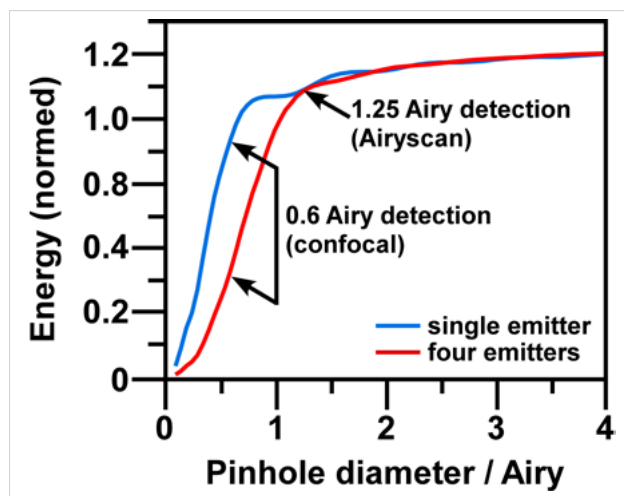


**Figure 8** Available energy in confocal microscopy. The graph shows simulations of the available energy, i.e. the number of photons, used for imaging in dependence of the pinhole diameter size (in AU) for the case of a single emitter (blue line) and four emitters (red line) in close proximity. Energy was normed to the value at 1 AU of the four emitter case. The energy distribution in case of one single emitter reflects the energy distribution of the Airy disk of a microscope's point spread function (PSF) in the lateral plane. In case of four emitters the curve is shifted to higher pinhole values until the point of saturation, that occurs at around 1.25 AU in both cases. The energies available for 0.6 Airy detection, used in a confocal, and 1.25 Airy detection used routinely in Airyscan are indicated by arrows.

### Photon Detection Considerations:

#### Airyscan vs LSM + DCV

The pinhole of a traditional LSM would need to be set to 0.2 AU in order to come near the resolution increase afforded by the Airyscan. This will work only for very bright and stable specimens that can be imaged with high laser powers to generate and detect enough photons in the image.

On the other hand opening the pinhole to 1 or 1.25 AU to match the amount of photons collected by the Airyscan will inadvertently lead to unwanted resolution loss that cannot be recovered in a subsequent DCV. Therefore the best strategy for traditional LSMs seems to be to restrain resolution loss by closing the pinhole to a suboptimal value (around 0.6 AU), where the loss in photon detection can be compensated for by slower sampling rates, and then deconvolving the image. Additionally, a quick review of theory would suggest imaging a single fluorophore with a traditional confocal system with a pinhole size of 0.6 AU would seem to maintain photon loss through the pinhole at a tolerable level such that the resulting image SNR should not degrade substantially (Fig. 8).

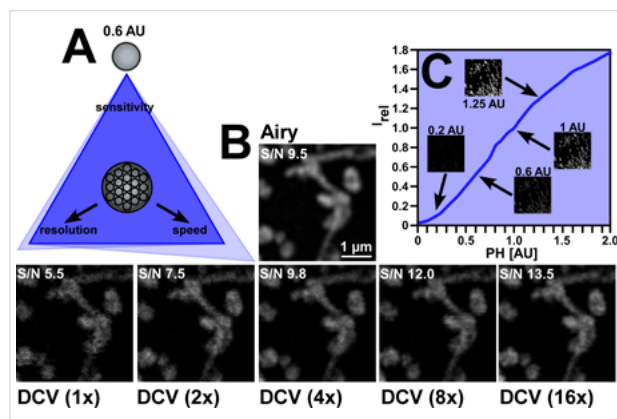


**Figure 9** Available energy in confocal microscopy at 0.60 AU. (A) Eternal triangle for confocal imaging at 0.6 AU. The slower scan speed to keep sensitivity will not fully compensate for a slight loss in resolution. Resolution can be increased further by slowing down acquisition speeds further. (B) Airyscan image (Airy; top) and deconvolved confocal images at the indicated averaging (DCV (1x) to DCV (16x); bottom row). The signal-to-noise ratios (SNR) of the raw Airy and confocal images before processing are indicated in the images. 4x averaging in the confocal lead to a comparable SNR of the summed phase image (resembling a confocal image) of Airyscan. Sample Fluocell #1 Thermo Fisher Scientific imaged for mitochondria stained with Mitotracker orange using a Plan Apochromat 63x / oil 1.4 objective lens and 561 nm excitation line at 0.2%. One plane was recorded. Image conditions for Airyscan were as follows: resolution 524 x 524, pixel (px) size 0.047  $\mu\text{m}$ , pinhole 1.25 AU, sampling rate 2.02  $\mu\text{s}/\text{px}$ . Variations for confocal: pinhole 0.6 AU and the indicated line wise mean averaging. Deconvolutions on confocal images were performed with regularized inverse filtering excluding a Stokes-vector. Scale bar is indicated in the Airyscan image. Images should be viewed at higher magnification in order to appreciate the differences in the noise contribution. (C) Relative intensities ( $I_n$ ) in dependence of the pinhole diameter in AU (PH [AU]) of Fluocells #1 confocal images. Selected images at 0.2 AU, 0.6 AU, 1 AU and 1.25 AU are displayed as indicated. The arrow indicates their related relative intensities. Intensities were normed to the value obtained at 1 AU. Image conditions using a Plan Apochromat 63x / oil 1.4 objective lens and 561 nm excitation line at 0.4% were as follows: resolution 512 x 512, pixel (px) size 0.051  $\mu\text{m}$ , sampling rate 1.52  $\mu\text{s}/\text{px}$ , pinhole size as indicated.

For a single emitter the energy loss from closing the pinhole from 1.25 AU to 0.6 AU is approximately 20% (Box 4). This can be compensated by 2x averaging. However, since in most biological samples many fluorophores are situated in proximity to one another, a more informative theoretical example would be to consider multiple fluorophores. In the case of four fluorophores, the loss in photon detection is dramatically higher amounting to around 65%, which would mean 4x - 8x averaging in order to match the SNR of a 1.25 AU image. A similar situation is seen with a real sample (Fig. 9). In the case study, the reduction in image intensity from 1.25 AU to 0.60 AU was approximately 60%, translating into 4x averaging. Closing the pinhole down to 0.2 AU is not practical as the loss in detected photons is too high (>90%).

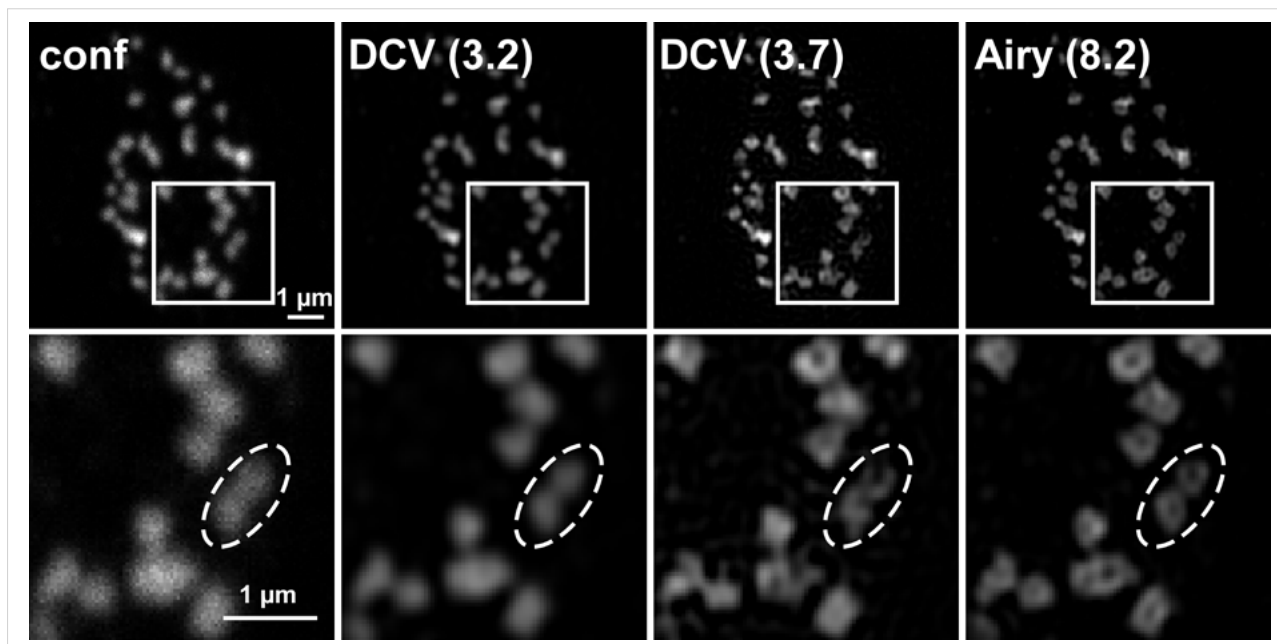


**Figure 10** Deconvolution (DCV) performance in Airyscan and confocal images. Bruchpilot (Brp) were imaged using a Plan Apochromat 150x / 1.35 Glyc objective lens and 488 nm excitation line at 0.5% with an Airyscan setup. Phase images were either summed to reconstitute the confocal image (conf) or used to calculate the Airyscan image (Airy). The confocal image was subsequently deconvolved (DCV) with the algorithms used in Airyscan. Hence the confocal and Airyscan images drew on the same raw data set. The upper panel shows overviews of a confocal image (conf), deconvolved confocal images at the indicated noise filter setting (DCV (3.2) and DCV (3.7)) and Airyscan image at the indicated noise filter setting (Airy (8.5)). The lower panel shows magnified parts of the boxed area of the upper panel images. Note that a noise filter setting of 3.2 (corresponding to a Wiener filter of 10-3.2) was not sufficient to resolve the structure. Noise filtering had to be decreased to 10-3.5 in order to obtain a resolution comparable to Airyscan. However, this was already associated with over- and undershoots of which the Airyscan image was devoid. Also artefacts in the DCV image are visible as denoted by the stippled oval. E.g. in DCV an open ring structure is observed that is closed in the Airyscan image, or the ring structure was not resolved as good as in Airyscan. Imaging conditions were as follows: resolution 1024 x 1024, pixel (px) size in x,y 0.037  $\mu\text{m}$ , z-section 0.125  $\mu\text{m}$ , pinhole 1.25 AU, sampling rate 0.73  $\mu\text{s}/\text{px}$ . The sample is *Drosophila melanogaster* larval sections stained for the pre-synaptic protein Bruchpilot (Brp) with Alexa 488 (scale bars indicated) and kindly provided by Jan Pielage, Friedrich-Miescher-Institute (FMI), Basel, Switzerland.

Therefore the strategy employed on traditional LSMs (closing the pinhole to a suboptimal value, around 0.6 AU, and then deconvolving the image) does not suitably address most biological samples. For weak fluorescent samples that undergo rapid photobleaching, live cell studies, or large z-stacks increasing laser exposure or slowing the sampling rate, in order to increase the number of photon detected is not an option due to negative impact of increased laser exposure or loss in temporal resolution.

### Airyscan and Deconvolution (DCV)

In order to understand why Airyscan supports deconvolution better than traditional confocal microscopy, it is helpful to remember the effect a microscope has on the collected fluorescence of single fluorophore. The collected fluorescence from a point emitter (single fluorophore) is convolved by the optics of a microscope (convolution), which leads to a blur effect. This blur effect is described by the point-spread function (PSF).

Deconvolution (DCV) tries to reverse the effects of convolution on the recorded data set and thus attempts to restore the original object information. DCV algorithms often employ theoretically calculated PSFs, due to the lack of knowledge about the actual properties of sample and imaging system. In addition, assumptions on the noise contribution have to be made when using DCV algorithms on traditional confocal images. However, if the type of noise is known, one might improve the estimate on the object through techniques such as Wiener deconvolution.

For the deconvolution of the Airyscan image a Wiener filter is used. Such a non-iterative linear algorithm has the advantage of producing a defined result. Iterative algorithms – typically used for DCV of traditional confocal images – have no known solution and thus come with a higher risk of miscalculating the true object structures (Box 7).

As stated previously, images acquired with the single detector elements of Airyscan are separately deconvolved.



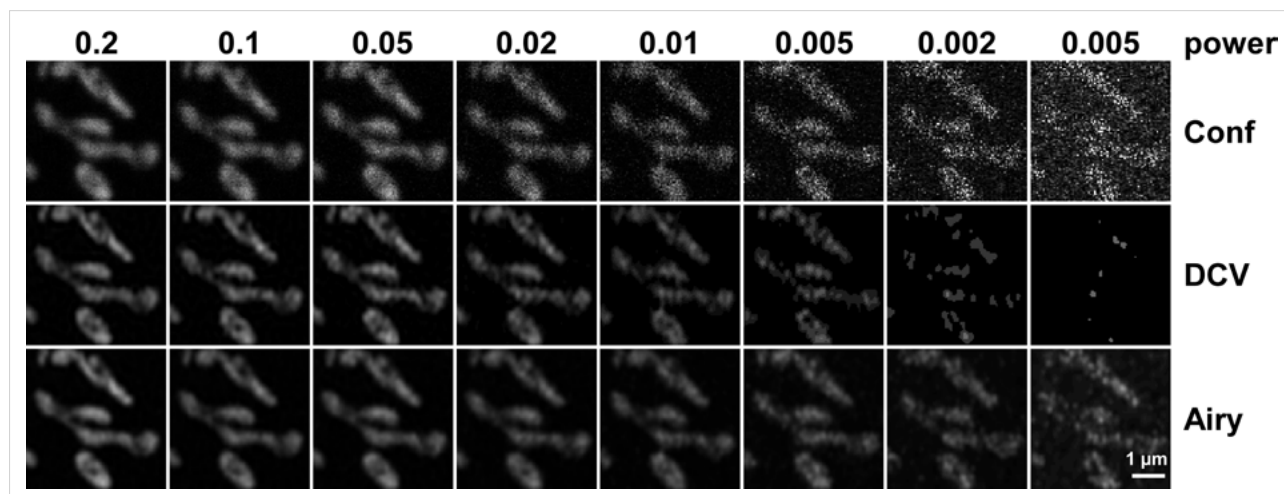


**Figure 11** Phase images were used to reconstruct a confocal image (Conf), a confocal processed with Airyscan (DCV) and the Airyscan image (Airy) at different laser power settings (values given a % of full power) to mimic increasingly less SNR along decreasing laser power. The sample was a FluoCell #1 (InVivoGen) stained for mitochondria with Mitotracker. Note that DCV fails to produce robust results even in images with less noise (laser power 0.02%) compared to Airyscan (starting with a laser power of 0.005%). Display curves were set to match brightness.

The contribution of each detector element is weighted according to the respective PSF. This makes the reassignment of the individual detector images part of the deconvolution process, therefore preserving not only the lateral, but also the axial resolution information (Box 8).

In general, since higher frequencies are contained in the individual detector element images, Airyscan is able to extend the effective resolution gains beyond the limit of the Sheppard sum. However, since the spatial contrasts are improved in the detector elements containing the higher spatial frequencies, the linear Wiener DCV utilized in Airyscan processing will be far more robust than any DCV implemented in combination with a traditional LSM image. In other words to achieve resolution near that of Airyscan, the confocal DCV will be more prone to artefacts and errors as it does not have access to the higher frequency information of Airyscan (Fig. 10). In addition, Airyscan processing is able to handle much noisier images than traditional deconvolution on a confocal image (Fig. 11).

### Summary

The growth and development of the laser scanning microscopy industry over the past 25 years has led to improvements that have been designed to increase image contrast

and instrument versatility. Utilizing foundation laid by Bertero [4] and Sheppard [5], the Airyscan detector from ZEISS replaced the most fundamental part of a traditional laser scanning microscope: the pinhole. The novel detector design of Airyscan dispenses with the classical physical pinhole and unitary detector assembly and utilizes a new pinhole-plane image detection assembly based on a collection of 32 detection elements. In the new assembly, each of the 32 detector elements acts as its own small pinhole with positional information. The positional information gained by the new approach allows for increased contrast of high spatial frequency information previously not available in traditional confocal systems. The increase in spatial frequency contrast enables Airyscan to produce images with substantially increased SNR and resolution compared to an LSM acquiring images with a 1 AU pinhole without having to increase laser exposure or sampling. Airyscan delivers 1.7x higher resolution in all three spatial dimensions and increases SNR by a factor of 4 – 8x, compared to traditional confocal LSM images acquired with a 1 AU pinhole.

Further, as a confocal detector Airyscan benefits from all advantages of confocal microscopy, above all out-of-focus light reduction. Hence Airyscan can work on optically dense samples, where other wide-field based superresolution techniques might fail.

## Box 1 Image formation in Confocal Microscopy

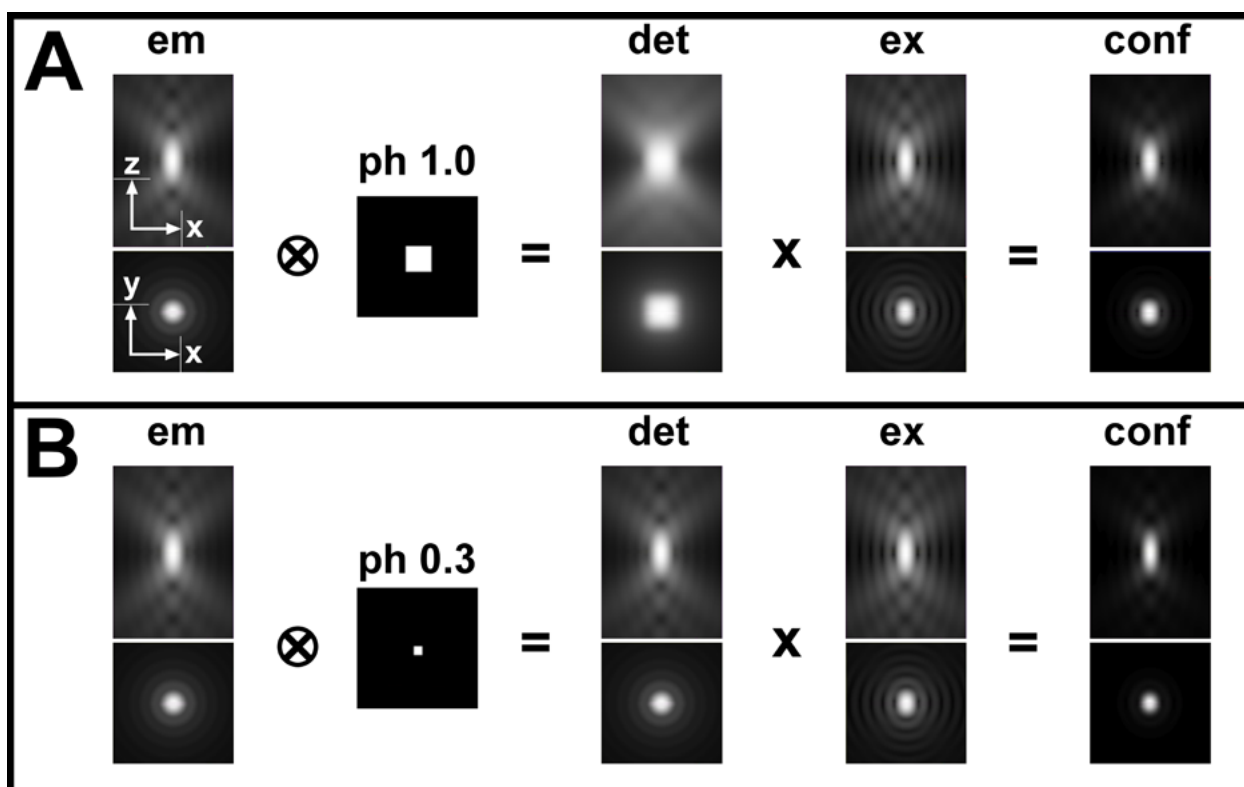


**Figure B1** (A, B) Image formation in a confocal microscope. The illumination PSF is generated by a focused laser beam and hence corresponds to the excitation PSF (ex). The emission PSF (em) on the other hand is convolved by the pinhole (ph) to form the detection PSF (det). The product of the detection PSF with the excitation PSF results in the confocal PSF (conf), which will be reduced in its lateral and axial extensions compared to the emission PSF, which would correspond to the wide-field PSF. A smaller pinhole size (0.3 AU in panel B compared to 1.0 AU in panel A) will lead to enhanced resolution, but with a drastic loss in detection efficiency. Simulations performed with  $NA = 1.4$ ; linear polarized light along x-axis for excitation, detection unpolarized;  $\lambda_{ex} = 488$  nm, no Stokes shift in emission. Gradation ( $\gamma$ ) in the pictures is 0.35.

The image in a confocal microscope is subjected to convolution of the emission PSF ( $PSF_{em}$ ) by the pinhole (PH) to form the detection PSF ( $PSF_{det}$ ) (formula 1). Since the detection PSF is multiplied by the illumination PSF ( $PSF_{illu}$ ) that corresponds to the excitation PSF ( $PSF_{ex}$ ) in a laser scanning microscope (LSM) the resulting confocal PSF ( $PSF_{conf}$ ) has a reduced full width at half maximum (FWHM) in the lateral direction. Besides a z-sectioning effect, z-resolution is improved as well. The theoretical possible narrowing by a factor of  $\sqrt{2}$  (if we

assume a Gaussian distribution of the detection and excitation PSFs and no Stokes shift in the emission) is only achieved if the Pinhole becomes a delta function, i. e. infinitesimally small. A infinitesimally small pinhole is impractical as no light would reach the detector. A pinhole size of 1 Airy unit (AU) represents a good compromise between resolution and signal strength. By closing the pinhole resolution will increase, however at a significant loss in signal.

$$(1) PSF_{conf}(r) = PSF_{illu}(r) \cdot PSF_{det}(r) = PSF_{exc}(r) \cdot (PSF_{em}(r) \otimes PH(d))$$

## Box 2 Resolution in Confocal Microscopy

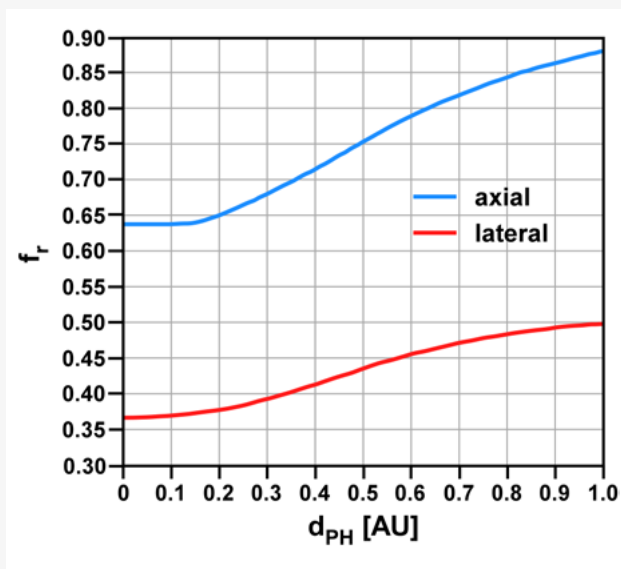


**Figure B2** Resolution factor  $f_r$  for axial (blue line) and lateral (red line) resolution in dependence of the pinhole diameter  $d_{PH}$  measured in Airy units (AU). Values of  $f_r$  at the extreme pinhole diameters of 0 and 1 can be analytically solved. For the lateral direction  $f_r(0)=0.37$  and  $f_r(1)=0.51$ ; for the axial direction  $f_r(0)=0.37$  and  $f_r(1)=0.51$ . Values for pinhole diameters between have to be numerically calculated.

If we define the resolution by the full width at half maximum (FWHM) the following relationships exist for the lateral (lat) and axial (ax) direction:

$$(1) FWHM_{lat} = f_r(d_{PH}) \cdot \frac{\bar{\lambda}}{NA} \quad \text{with} \quad \bar{\lambda} = \sqrt{2} \cdot \frac{\lambda_{ex} \lambda_{em}}{\sqrt{\lambda_{ex}^2 + \lambda_{em}^2}} \approx \sqrt{\lambda_{ex} \cdot \lambda_{em}}$$

$$(2) FWHM_{ax} = f_r(d_{PH}) \cdot \frac{\bar{\lambda}}{(n - \sqrt{n^2 - NA^2})} ; \text{ for } NA < 0.5:$$

$$FWHM_{ax} \approx f_r(d_{PH}) \cdot \frac{n \cdot \bar{\lambda}}{NA^2}$$

Parameters: FWHM: full width at half maximum,  $f_r$ : resolution factor,  $d_{PH}$ : pinhole diameter, NA: numeric aperture of objective, n: refractive index of medium,  $\bar{\lambda}$ : weighted excitation (ex) and emission (em) wavelength

## Box 3 Principle working of the Airyscan detector

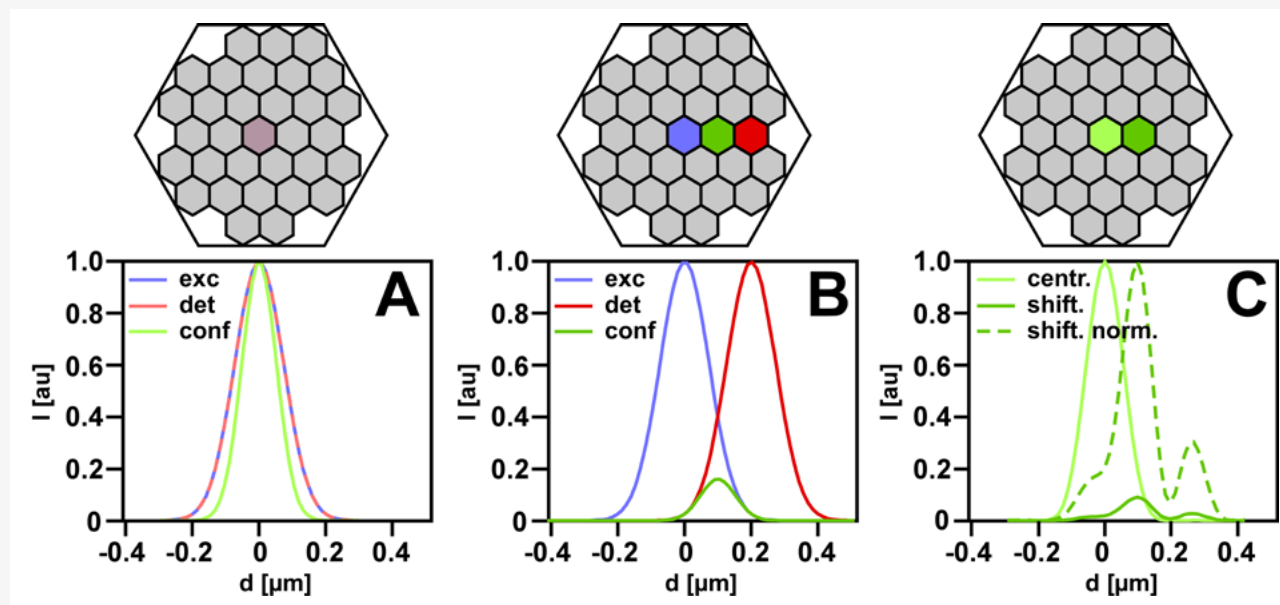


**Figure B3** Confocal lateral PSF in Airyscan. The confocal PSF (conf) is the product of the excitation PSF (exc) with the detection PSF (det). For a central (centr.) located detection element the maximum of the product is also centered (A). Assuming a Gaussian profile for both PSFs as an approximation and no Stokes shift the confocal PSF will be narrowed by a factor of  $\sqrt{2}$  compared to the excitation and detection PSF. For a shifted detector element (shift.) the maximum of the confocal PSF is lowered in intensity and shifted as well (B). Assuming a Gaussian profile the shift will be half the distance between the central and shifted detector element. As before, the confocal PSF will be narrowed by a factor of  $\sqrt{2}$ . Assuming a more realistic Bessel function for the PSFs the resulting confocal PSF gets increasingly steep with increasing shift between excitation and emission. The side lobes do no harm when treated by the deconvolution properly. In total, all detector elements contribute to improved resolution and contrast. The shifted elements contribute even more than the central element, with respect to their intensity.

Simulations were done with  $\lambda = 488 \text{ nm}$ , no Stokes shift;  $\text{NA} = 1.4$ ; PSF approximation by Gaus function in panels A & B and by Bessel function in panel C.

As the confocal PSF is the product of the excitation and detection PSFs it will be narrowed by a factor of  $\sqrt{2}$  assuming a Gaussian function for the PSFs (equations 1 and 2). If the maximum of excitation and detection PSFs are centrally located, so will be the maximum of the confocal PSF (equation 1). However, if the detection element is shifted by a distance  $x_0$ , the maximum of the confocal PSF is shifted by half that distance, i. e.  $x_0/2$  (equation 2). Assuming a Bessel function for the PSFs, the narrowing of the confocal PSF is

$$(1) \text{PSF}_{conf}^G = \text{PSF}_{exc}^G(x) \cdot \text{PSF}_{det}^G(x) = e^{-\frac{x^2}{\sigma^2}} \cdot e^{-\frac{x^2}{\sigma^2}} = e^{-\frac{2 \cdot x^2}{\sigma^2}} = e^{-\frac{x^2}{(\sigma/\sqrt{2})^2}} \text{ with } \sigma = \text{standard deviation}$$

$$(2) \text{PSF}_{conf}^G = \text{PSF}_{illu}^G(x) \cdot \text{PSF}_{det,x_0}^G(x) = e^{-\frac{x^2}{\sigma^2}} \cdot e^{-\frac{(x-x_0)^2}{\sigma^2}} = e^{-\frac{2 \cdot (x-x_0/2)^2 + x_0^2}{\sigma^2}} = e^{-\frac{x_0^2}{4}} \cdot e^{-\frac{(x-x_0/2)^2}{(\sigma/\sqrt{2})^2}}$$

$$(3) \text{FWHM} = 2 \sqrt{2 \ln 2} \cdot \sigma$$

more pronounced. With  $\lambda = 488 \text{ nm}$  and an  $\text{NA} = 1.4$ , the full width at half maximum (FWHM) of the central confocal PSF amounts to 130 nm (the FWHM can be computed from the standard deviation  $\sigma$  of a gauss function according to equation 3); for the shifted PSF it is ca. 104 nm. Hence, the shifted detector elements contribute disproportionate to resolution enhancement, but the overall effect is small compared to the contribution of a drastically increased SNR.

## Box 4 Energy considerations

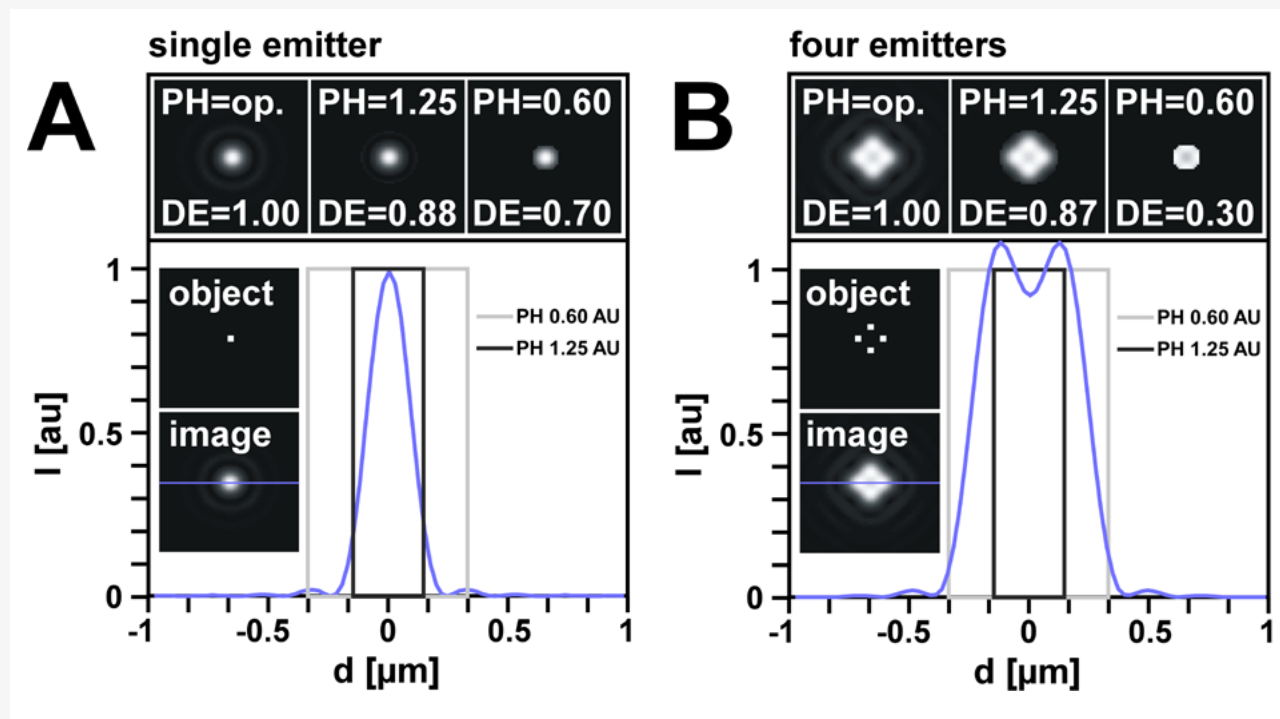


**Figure B4** Detection efficiencies in confocal imaging. The upper panel shows detection efficiencies (DE) in normed units with the pinhole (PH) open (op.), or at 1.25 and 0.60 AU in the case of a single emitter (A) or four emitters (B) in simulations for a stationary beam (no scanning). The lower panel shows the positions of the emitters in the object plane and the image or detection plane. The cross section of the emitter signal (thick blue line) in the image plane (indicated by the thin blue line) is plotted with intensity ( $I$ ) in arbitrary units (au) versus distance ( $d$ ) in micrometer ( $\mu\text{m}$ ). The extent of the covered signal at pinhole sizes of 1.25 and 0.60 Airy Units (AU) are indicated by the dark and light grey boxes, respectively.

Closing down the pinhole will result in increasing light loss. In the case of a single emitter. For a single emitter light detection efficiencies at pinhole sizes of 1.25 and 0.60 AU are still reasonable (about 88% and 70% of the signal with an open pinhole). However, the situation is dramatically changed for multiple emitters. In the case of four emitters, simulations show that light losses at 1.25 AU are still confined (87% signal compared to an open pinhole) but are

drastically reduced to 30 % in the case of a pinhole set at 0.6 AU. The latter scenario represents the situation with stained samples, where fluorescent emitters are usually dense. In this case only collecting more photons by slower scanning or averaging as well as increasing laser power can compensate for the loss in signal-to-noise, which are, however, all measures impinging negatively on live cell imaging.

## Box 5 xy-resolution in Airyscan

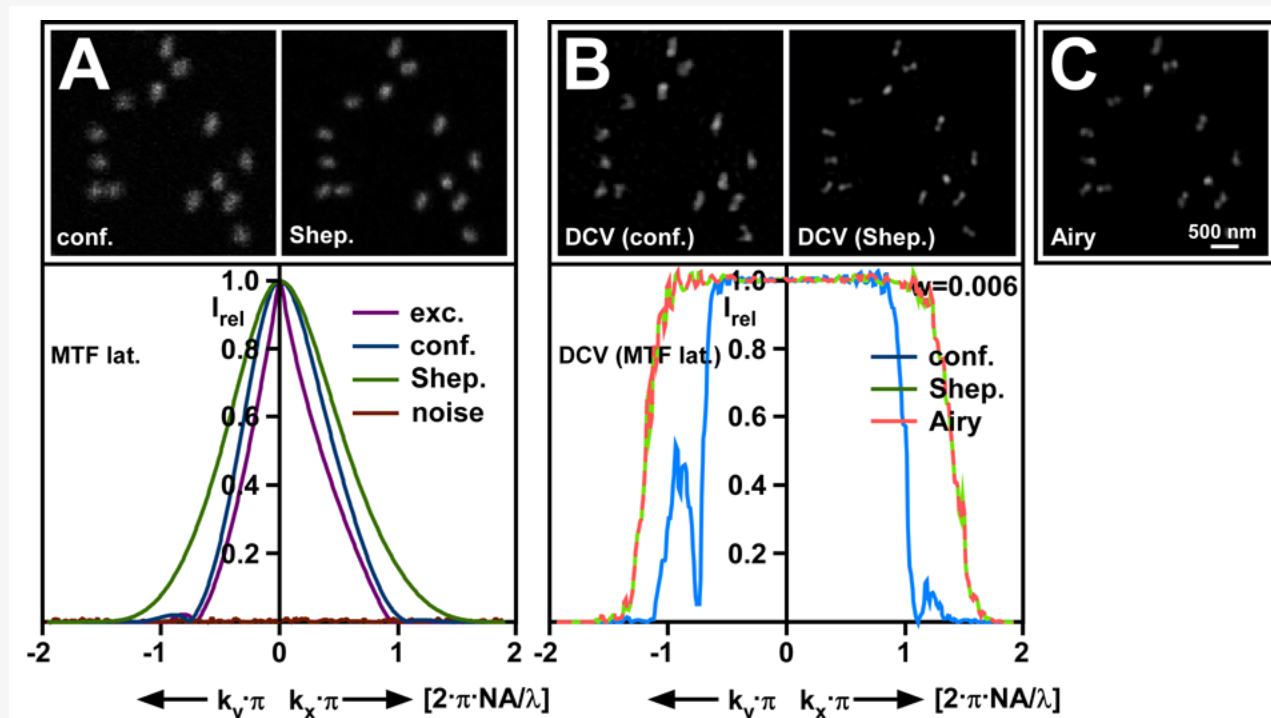


**Figure B5** Lateral Modulation Transfer Function (MTF) and resolution. (A) The upper panel shows a confocal (conf.) and a Sheppard sum (Shep.) image of 140 nm Origami sample (GATTAquant, Germany). The lower panel shows the MTF of the imaging setup. The confocal MTF already shows slightly improved contrasts as compared to the excitation MTF alone. Which means, contrast is slightly improved, compared to a wide field microscope or an LSM with open pinhole. Using the Airyscan detector the MTF is both raised in intensity and extended to higher frequencies. This is depicted by the Sheppard MTF. The effective “hardware” MTF for Full DCV Airyscan will be the same as the Sheppard MTF for the lateral case.

(B) The same images and MTFs with deconvolution. The target of deconvolution is to raise all contrasts to unity level. Which means, the contrast of structures is not altered, giving an image with optimized resolution as close to the original sample as possible.

Image noise is distributed evenly over all spatial frequencies. The noise level limits the frequency range in which the MTF could be raised. Since the “raw” or “hardware” MTF of the Airyscan detector is widely extended over the confocal MTF, the final Airyscan image benefits from deconvolution far more than the deconvolved confocal image. This can be clearly seen in the images above.

Plot Simulations were done with  $\lambda_{exc}=488$  nm light linear polarized along the x-axis as well as unpolarized light for detection with no Stokes shift; NA=1.4 and pinhole size of 1.25 AU.

The modulation transfer function (MTF) is the amplitude of the optical transfer function OTF (equation 1), which is the Fourier transform of the point spread function (PSF).

The MTF describes the achievable contrast in the image.

The MTF in a confocal is enlarged compared to the excitation or detection MTFs in the lateral direction as they convolve each other (equation 2). In the Sheppard sum, the MTF is substantially expanded in the lateral direction (panel A),

$$(1) \quad MTF(\omega) = |OTF(\omega)|$$

$$(2) \quad OTF_{conf}(k_r) = OTF_{illu}(k_r) \otimes OTF_{det}(k_r)$$

which is also evident in the Sheppard sum image, which shows higher SNR and resolution than the confocal image. This more on higher frequencies helps in deconvolution to raise their amplitudes above what is achievable for a confocal image (panel B). The Sheppard sum shows a resolution enhancement in the lateral direction of about 1.4 fold. In total, however, a resolution enhancement of a factor of 1.7 can be achieved in the lateral direction.

## Box 6 z-resolution in Airyscan

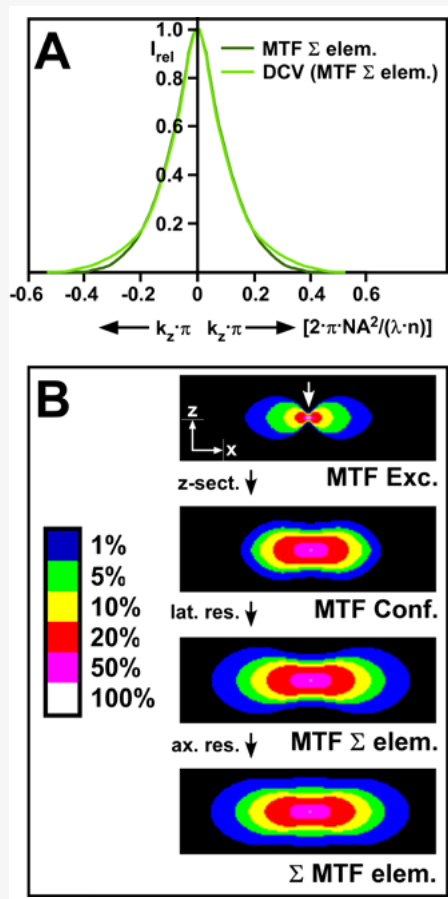


**Figure B6** 3D Modulation Transfer Function (MTF)

(A) MTF in z-direction (as indicated by the arrow in inset (B), 1<sup>st</sup> image) This MTF shows the ability of the LSM to distinguish between z-planes and is directly related to the sectioning capability. The blue graph shows the axial MTF of the standard confocal setup. It would be exactly the same for a sheppard sum image. The green graph shows the effective "hardware" MTF of the Airyscan full DCV which is extended over the conventional MTF. Deconvolution would raise frequencies as long as allowed by noise, the same way as described in Box 5.(B) xz cross section MTFs for increasingly sophisticated imaging approaches.

1. Excitation or Wide field PSF, conventional lateral resolution, missing cone in z-direction as indicated by arrow which means this MTF does not show any sectioning capabilities.
2. Confocal MTF . Basically the same lateral resolution as in wide field, however the missing cone is almost removed. The confocal MTF can section images.
3. Sheppard Sum MTF. Laterally extended over the confocal approach, the sectioning capability is the same as for conventional confocal imaging.
4. Airyscan DCV . The remains of the missing cone are also removed, leading to an even improved optical sectioning capability.

Calculation parameters: The plot shows relative intensities ( $I_{rel}$ ) versus inverse distance in z ( $k_z$ ); 1 unit corresponds to  $5,7 \mu\text{m}^{-1}$  for  $\lambda_{ex}=488 \text{ nm}$  & NA 1.4 (B) 3D simulation of MTF of excitation PSF(MTF Exc.), confocal PSF (MTF Conf.), Sheppard sum (MTF  $\Sigma$  elem.) and sum of MTFs of each detector element at pinhole size = 1.25 AU. The excitation MTF is not normed to the confocal MTFs (Conf., sum elements, sum MTF elements), which are normed to each other. The missing cone is indicated by the arrow.

The missing cone of the excitation MTF is partly filled in in the confocal MTF resulting in better sectioning capability (panel B). The Sheppard sum (the sum of the back shifted detector elements) extends in the lateral direction compared to the confocal and therefore displays higher lateral resolution; but there is no extension in the axial direction, so no further improvement in z-resolution compared to the confocal can be expected; only that the MTFs of the Sheppard sum will be less

noisy. However, if the MTF of each detector element is taken and the MTFs summed, the missing cone is filled in further. Axial resolution enhancement can be achieved if the signals from the different detector elements are separately deconvolved (panel B). As this effect is slight, the major resolution gain in z stems from the DCV (panel C). In total, a resolution enhancement of a factor of 1.7 and even higher dependent on the optical density of the sample can be achieved.

## Box 7 Deconvolution (DCV)

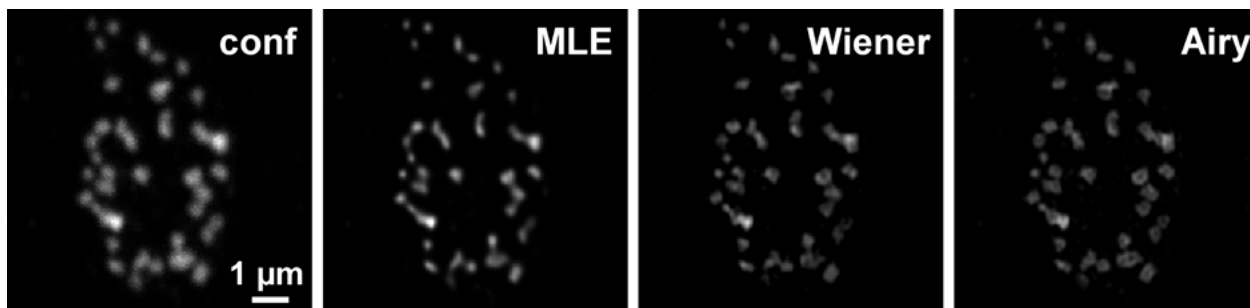


**Figure B7** Deconvolution of a confocal image (conf) by Maximum likelihood estimation (MLE), Wiener filtering (Wiener) and Airyscan also implying a Wiener filter to the individual signal contribution of the Airyscan detector elements (Airy). The iterative approach by MLE failed to accurately restore the object structures in contrast to the linear Wiener filtering. As Airyscan provides positional information, its reconstructed image is the best representation of the object structure of the used DCV methods.

In a general meaning deconvolution is an algorithm-based process used to reverse the effect of convolution on recorded data. Specifically in optics and imaging the term refers to reversing the optical distortions that take place in an imaging instrument to obtain clearer images. Hereby the object  $O(r)$  is convolved by the effective point spread function (PSF)  $EH(r)$  to yield the image  $D(r)$  (equation 1). The problem is to determine the unknown function  $O(r)$  through the known measured function  $D(r)$  and transfer function  $EH(r)$ , known as the inverse convolution problem [4]. One solution approach offers the convolution theorem according to which the Fourier transform of a convolution of two functions equals the product of the Fourier transforms of the two individual functions (equation 2). By this relation  $\hat{O}(\omega)$  can in principle be determined by a simple division (equation 3, followed by reverse Fourier transformation, a procedure known as inverse filtering (deterministic deconvolution). However this rule is not generally applicable. First  $\hat{O}(\omega)$  might not be unambiguous; second,  $\hat{EH}(\omega)$  could contain zeros and third, real data can be afflicted with additive noise  $N(r)$  or  $\hat{N}(\omega)$ , respectively, so that the problem complicates (equations 4 and 5). For that reason diverse procedures are employed that aim to determine the most likely outcome for  $O(r)$ , since an unambig-

uous analytical solution does not exist. When the PSF is not known one could potentially deduce it by systematically trying different possible PSFs whilst assessing the improvements in the image (blind deconvolution). The lower SNR, the worse the estimate of the deconvolved signal will be. The noise  $\hat{N}(\omega)$  would be disproportionately amplified using the division procedure of inverse filtering (equation 6). Noise amplification is a direct result of the fact that  $\hat{EH}(\omega)$  will usually decline towards zero at high frequencies, whereas noise contains in that frequency band components that would be amplified by the division. That is the reason why inverse filtering often provides not a sufficient solution. However, if we have at least some knowledge of the type of noise in the data (e. g. Poissonian noise, Gaussian noise etc.), the estimate of  $O(r)$  can be greatly improved through techniques such as Wiener deconvolution, which is the most common non-iterative algorithm. Iterative methods, like the Richardson-Lucy deconvolution or deconvolution base on Maximum Likelihood estimations (MLE), are model-based and hence no unique solution exists. They might provide better resolution but are on the other hands more prone to erroneous results. Regularization in iterative algorithms or inverse filtering can be applied to avoid unrealistic solutions.

$$(1) \quad D(r) = O(r) \otimes EH(r)$$

$$(2) \quad \hat{D}(\omega) = \hat{O}(\omega) \cdot \hat{EH}(\omega)$$

$$(3) \quad \hat{O}(\omega) = \hat{D}(\omega) / \hat{EH}(\omega)$$

$$(4) \quad D(r) = O(r) \otimes EH(r) + N(r) \quad \text{or}$$

$$(5) \quad \hat{D}(\omega) = \hat{O}(\omega) \cdot \hat{EH}(\omega) + \hat{N}(\omega)$$

$$(6) \quad \hat{O}(\omega) = \hat{D}(\omega) / \hat{EH}(\omega) + \hat{N}(\omega) / \hat{EH}(\omega)$$



## Box 8 Deconvolution (DCV) by linear Wiener filtering in Airyscan

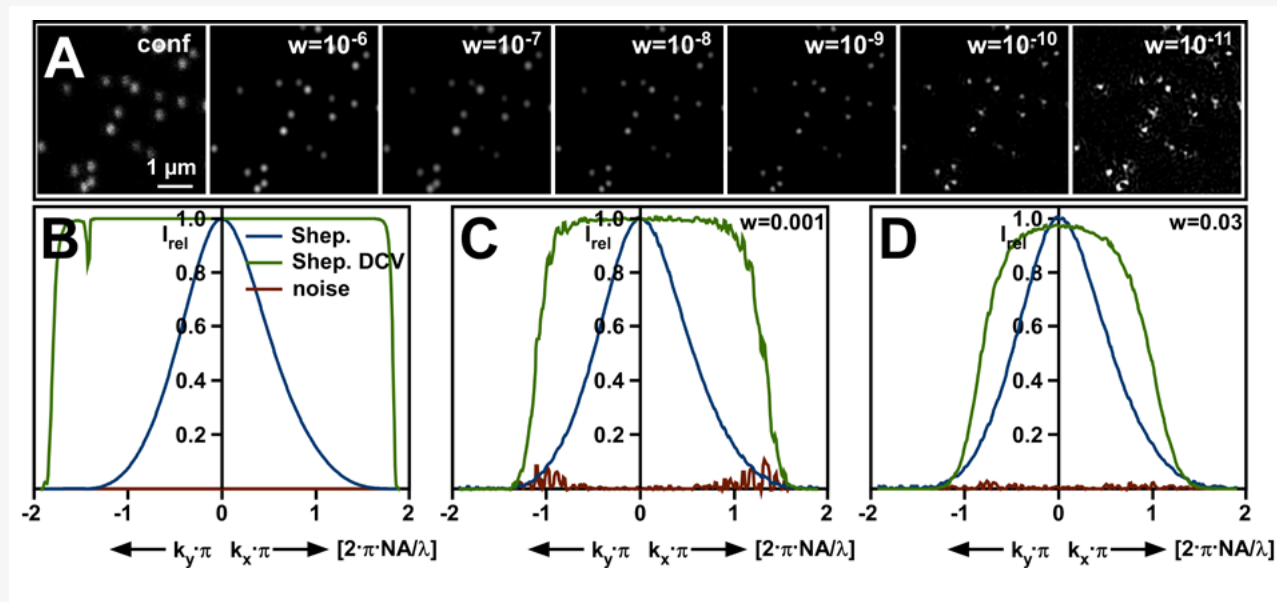


**Figure B8** Deconvolution by Wiener linear filtering. (A) 100 nm TeraSpek beads imaged with a confocal (conf) and subsequently deconvolved by Wiener filtering using the indicated Wiener noise filter. (B-D) MTF of Sheppard sum before (Shep.) and after (Shep. DCV) deconvolution without added noise and with added noise using a Wiener parameter ( $w$ ) of 0.001 (C) and 0.03 (D). 1 unit corresponds to  $5,7 \mu\text{m}^{-1}$  for  $\lambda=488 \text{ nm}$  excitation and NA 1.4.

If deconvolution is performed with linear Wiener filtering, the choice of the Wiener noise filter will balance between higher resolution and better SNR in the image.

The smaller the filter will become, the higher the resolution, but the more will noise interfere with a good SNR.

If noise is not removed by the filter, it will create artefacts in the form of over- & undershoots as well as ringing and honeycomb structures (A). If noise is removed, the MTF will become narrower, i. e. higher frequencies are not as much amplified any longer (B-D).

For Airyscan deconvolution by Wiener linear filtering, the signal of each detector element is deconvolved separately and the contribution of each detector element is weighted (equation 1). This allows for a better and more robust DCV as the positional information of the detector elements will be taken into account. The Wiener parameter ( $w$ ) is the squared

absolute amount of the noise spectrum divided by the squared absolute amount of the object spectrum (equation 2).

$$(1) \quad \hat{O}(\omega) = \frac{\sum_i^n (\hat{D}_i(\omega) \cdot \hat{E}H_i^*(\omega))}{w + \sum_i^n |\hat{E}H_i(\omega)|^2}$$

$$(2) \quad w = \frac{\langle \hat{N}(\omega) \rangle^2}{\langle \hat{O}(\omega) \rangle^2}$$

Parameters:  $\hat{O}(\omega)$ : object spectrum;  $\hat{D}(\omega)$ : image spectrum, which is the measured signal;  $\hat{N}(\omega)$ : noise spectrum,  $\hat{E}H_i^*(\omega)$ :  $\text{OTF}_{\text{eff}}$ , star denotes complex conjugated function, which represents the phase correction;  $|\hat{E}H_i(\omega)|^2$ :  $|\text{OTF}_{\text{eff}}|^2$ ; which represents amplitude correction;  $i$ : index of detector elements;  $n$ : number of detector elements;  $w$ : Wiener parameter, which accomplishes noise suppression by setting the bandwidth limit.

**Cover image:**

SKBR3 cells, showing single RNA molecule FISH, detecting Her2 mRNA (green; Quasar 570 labeled) and Akt1 mRNA (red; Quasar 670)  
Courtesy of Sunjong Kun, Department of Biomedical Engineering, Oregon Health & Science University (OHSU), USA

---

**References:**

- [1] Conchello, J.-A. and J.W. Lichtman, Optical sectioning microscopy. *Nature methods*, 2005. 2(12): p. 920–931.
- [2] Minsky, M., Memoir on inventing the confocal scanning microscope. *Scanning*, 1988. 10(4): p. 128–138.
- [3] Neu, T.R. and J.R. Lawrence, Innovative techniques, sensors, and approaches for imaging biofilms at different scales. *Trends in Microbiology*, 2015.
- [4] Bertero M., Brianzi P., Pike E.R., Super-resolution in confocal scanning microscopy. *Inverse problems*, 1987. 3: p. 195–212
- [5] Sheppard, C.J., Super-resolution in confocal imaging. *Optik*, 1988. 80(2): p. 53–54.
- [6] Shotton, D.M., Robert Feulgen Prize Lecture 1995. Electronic light microscopy: present capabilities and future prospects. *Histochem Cell Biol*, 1995. 104(2): p. 97–137.
- [7] Sheppard, C.J., S.B. Mehta, and R. Heintzmann, Superresolution by image scanning microscopy using pixel reassignment. *Opt Lett*, 2013. 38(15): p. 2889–2892.



**Carl Zeiss Microscopy GmbH**  
07745 Jena, Germany  
microscopy@zeiss.com  
www.zeiss.com/microscopy



We make it visible.